Medical Image Analysis 71 (2021) 102043

Contents lists available at ScienceDirect

Medical Image Analysis

journal homepage: www.elsevier.com/locate/media

RICE: A method for quantitative mammographic image enhancement

Faraz Janan[a,*], Michael Brady[b]

[a] School of Computer Science, University of Lincoln, Issac Newton Building, Bradyford Pool LN6 7TS, United Kingdom
[b] Department of Oncological Imaging, University of Oxford, Old Road Campus Research Building, Headington, Oxford OX3 7DQ, United Kingdom

ARTICLE INFO

Article history:
Received 3 July 2020
Revised 9 March 2021
Accepted 15 March 2021
Available online 26 March 2021

Index Terms:
Image Enhancement
Contrast Enhancement
Breast Cancer
Cancer Masking
Breast Density
Focal Density

ABSTRACT

We introduce Region of Interest Contrast Enhancement (RICE) to identify focal densities in mammograms. It aims to help radiologists: 1) enhancing the contrast of mammographic images; and 2) detecting regions of interest (such as focal densities) that are candidate masses potentially masked behind dense parenchyma. Cancer masking is an unsolved issue, particularly in breast density categories BI-RADS C and D. RICE suppresses normal breast parenchyma in order to highlight focal densities. Unlike methods that enhance mammograms by modifying the dynamic range of an image; RICE relies on the actual tissue composition of the breast. It segments Volumetric Breast Density (VBD) maps into smaller regions and then applies a recursive mechanism to estimate the 'neighbourhood' for each segment. The method then subtracts and updates the neighbourhood, or the encompassing tissue, from each piecewise constant component of the breast image. This not only enhances the appearance of a candidate mass but also helps in estimating the mass density. In extensive experiments, RICE enhances focal densities in all breast density types including the most challenging category BI-RADS D. Suitably adapted, RICE can be used as a precursor to any computer-aided diagnostics and detection system.

1. Introduction

Brest cancer is the second most frequently diagnosed cancer in women. In 2020, in the USA alone, there will be an estimated 276,480 new cases of breast cancer in women (and 2620 in men), with a projected 42,690 deaths (Siegel et al., 2020). This continues the increase over 2017 (252,710 new cases and 40,610 breast cancer deaths) (DeSantis et al., 2017). Breast cancer accounts for 30% of all female cancers. In the developed world it is the second leading cause of cancer death among women (after lung cancer), whereas it is the leading cause in less developed countries(Romualdo et al., 2013; Siegel et al., 2015)(Torre et al., 2015). Early diagnosis improves prognosis, reduces the cost of treatment, and increases available treatment options. As well, it is estimated that for the year 2020-21 there will be an overall 27% increase in the cost of cancer care in the US, raising spending from $124.57Bn to $157.77Bn. Specifically, the cost of breast cancer care is set to increase by 32%. In response to all of these developments, better and more cost-effective imaging techniques, including reliable image enhancement methods, are crucial for maintaining or even reducing the economic burden of breast cancer.

Though a range of imaging modalities are used in clinical practice for the detection and work-up of breast cancer, including ultrasound, MRI, CT, and Tomo(synthesis) DBT, it remains the case that digital x-ray mammography is overwhelmingly the most commonly used. It is the basis for all state and privately funded screening programs in the UK, US, EU and beyond. Such a program has helped the UK attain the second-lowest predicted breast cancer mortality rate in 2020 (after Spain), starting from the highest one in 1970 (Tabár & Dean, 1982)(Carioli et al., 2017). Mammography is relatively low-cost, practical for large population screening, and there is strong evidence that it has decreased the mortality rate of breast cancer by more than 30% (Tabár et al., 2011).

To motivate the method introduced in this paper, screening mammography depends critically on the visibility of tumours, which may be surrounded by adipose or fibroglandular tissue. The appearance of a mammogram, considered as an image, varies considerably among women and depends upon the imaging parameters, tissue characteristics, and the response of different breast tissues to x-ray attenuation. Dense tissue, such as tumours and stromal tissue, has high x-ray attenuation and appears bright on a mammogram. Similarly, fatty tissue has low attenuation and appears dark. However, since mammography is projective, tumours may be partly or completely concealed by normal dense stromal tissue, and the greater the amount of such tissue, the greater the risk that a tumour may be "masked". Not only may bright stromal tissue mask a tumour, but it also reduces image contrast, fur-

* Corresponding author.
E-mail addresses: fjanan@lincoln.ac.uk (F. Janan), mike.brady@oncology.ox.ac.uk (M. Brady).

https://doi.org/10.1016/j.media.2021.102043
1361-8415/

ther increasing the challenge of detecting abnormalities in a dense breast. Mammography is currently estimated to miss 20% of invasive breast cancers, a number which may be reduced by the use of computer-aided detection or diagnostic systems (Le et al., 2019)(Sasaki et al., 2020)(Rodríguez-Ruiz et al., 2019); but such algorithms also tend to have a poorer performance for dense breast (e.g. BI-RADS 4). Women with dense breast not only have a higher risk of their breast cancers being missed at screening; but are also at significantly higher risk of developing breast cancer(Schreer, 2009)(Ghosh et al., 2012)(Van Goethem et al., 2004). In short, it is often difficult to detect Regions of Interest (ROIs) that may correspond to a lesion and to assess regional morphology.

In this paper, we propose a method based on the breast contents to improve the visibility of potential ROIs by adaptively and iteratively enhancing the contrast to their surroundings. We show its effectiveness by applying it to a database of mammograms assembled for the European project ASSURE (Adapting Breast Cancer Screening Strategy Using Personalised Risk Estimation,) and converted to quantified Volumetric Breast Density (VBD) maps by the Volpara Health software (Highnam et al., 2010; Teo et al., 2016). We note that there are no structural differences between a regular mammogram (intensity map, where each pixel carries an intensity value representative of the tissue x-ray attenuation) and a VBD image. Using density maps as we do enables confirmation that the regions enhanced by our method are indeed dense (Volpara density values per pixel), and thus are 'focally dense'. Along with the contrast enhancement of a mammogram, we particularly aim to enhance the visibility of cancers that are potentially masked behind dense parenchyma.

This paper is based on our previous work (Faraz Janan et al., 2015), in which we proposed a basic system for the region of interest enhancement, which has been significantly enhanced.

1.1. Masking and focal densities

Masking in relation to mammographic density remains one of the most challenging issues in diagnostic mammography. Complex patterns formed by focal densities, those linked to masking, result from multi-layered and multi-oriented tissue composition in mammographic images(Aiello et al., 2005). To date, detecting masking has been largely beyond human visual perception. Masking conceals tumours and obscure associated cancerous texture, making it difficult to detect cancers at an early stage particularly in dense breast(Chiu et al., 2010). We contend that focal densities are key to enabling the detection of masked tumours and establish focal asymmetry along with its subtypes. It is core to the guidelines on breast cancer screening issued by the American College of Radiology (ACR) in the BI-RADS 5th edition. The BI-RADS lexicon is a dictionary of descriptive terms used to describe a mammographic, ultrasound, or MRI finding (Spak et al., 2017). These protocols are used in routine clinical practice worldwide.

Increasingly, MRI is suggested to find cancers in dense breast (Longo, 2019). Van Gils (Bakker et al., 2019) showed in the DENSE trial that interval cancers are more common in dense breast for which there is a higher chance of cancer masking. The study showed that supplemental MRI screening reduced the interval-cancer rate from 5.0 per 1000 screenings in the control group to 2.5 per 1000 screenings in the MRI-invitation group. Whereas it reduced the interval-cancer rate in the supplemental MRI group by 1.3 per 1000 person-years. MRI also produced a reduced false-positive rate of 8% (79.8 per 1000 screenings) and only 26.3% of patients who had a breast biopsy following MRI had breast cancer. However, routine supplemental MRI investigations are infeasible primarily because of the relatively limited availability of MRI scanners and heavy usage that is made of them. This is compounded in many parts of the world by the higher cost of an MRI (typically 4-5 times that of a mammogram). For all of these reasons, we have investigated mechanisms to identify focal densities that are potential tumours masked behind dense parenchyma and whose clinical uses would include as a stratification step in the diagnostic pathway.

Statistical and texture based measures have been used to quantify cancer masking. Karssemeijer et al. (Holland et al., 2017) used percent density area (PDA), percent density volume (PDV) and the dense tissue masking model (DTMM) to assess the risk of cancer masking. They used 111 interval cancers collected over a period of 12 months after the initial examination against 1110 selected normal cases without cancer. Based on statistical measures they categorised women into high-medium-low risk categories. Yaffe et al. (Mainprize et al., 2019) used a cohort of 67 nonscreen-detected (detected via other means after a negative mammogram) and 147 screen-detected cancers invasive cancers A mechanism was devised to study the distribution of dense tissue using statistical and texture measures. They achieved an AUC of 0.75 [0.67–0.82] for predicting the risk of masking while using logistic regression. Both of these studies applied their models to Volpara volumetric density maps similar to those that we have used in our study. Yaffe et al. (Mainprize et al., 2014)(Alonzo-Proulx et al., 2019) also developed quantification metrics for possible use in stratified breast cancer screening using masking risk predictions. However, this was not aimed at improving the visibility of masked tumours, or unmask and quantify ROIs.

In this paper, we extend our previously-reported Region of Interest Contrast Enhancement (RICE) method to identify focal densities in mammograms. RICE finds focal densities by enhancing the appearance of dense tissue in mammograms. When applied to a density map (in the present case, generated by Volpara's breast density algorithm, VBD, though the method is applicable to any such density map), it also gives an approximation of the mean tissue density of an ROI. It generates a mammogram with contrast-enhancement.

Our method is perhaps best compared with contrast enhancement methods, most notably CLAHE (Constrast-Limited Adaptive Histogram Enhancement), that have been widely applied to mammograms. Such enhancement methods manipulate the intensity (or density) histogram, modifying the dynamic range, scaling of regional or global intensities histograms, and/or adjusting the contrast window of a digital mammogram (Akila et al., 2015). Histogram-based methods adapt the histogram of the entire image (or a segmented portion thereof), rather than analysing local regions that may correspond to focal densities.

In contrast, RICE suppresses normal parenchyma, irrespective of: the intensity distribution, the BI-RADS classification (if known), and texture information in an image. Applied to density maps, it estimates the overall density for all regions inside the breast that are not considered 'normal' parenchyma (relative to that breast); such as masses, highly dense tissue, and structural spicules or stromal ducts. RICE facilitates finding ROIs in dense breast, where established segmentation methods struggle. Fig. 1 shows a false-colour representation of the application of RICE to the (noisy) surface of a VBD map. The ROI becomes a candidate mass, enhanced when we subtract the normal parenchyma or surrounding tissue. The upper image shows the VBD surface before applying RICE. The lower image shows the image enhanced by RICE. The vertical axis shows the amount of dense breast tissue at each location (x,y). The peak highlighted in red is a mass that has a maximum density of 12mm in the original image. After applying RICE, the density of the mass reduces closer to 5mm due to subtraction of the normal parenchyma surrounding it. The overall density of the mass has reduced to represent its actual composition; however, its appearance has been considerably enhanced. Note that the second thin, sharp spike to the left of the mass is an enhanced microcalcification.

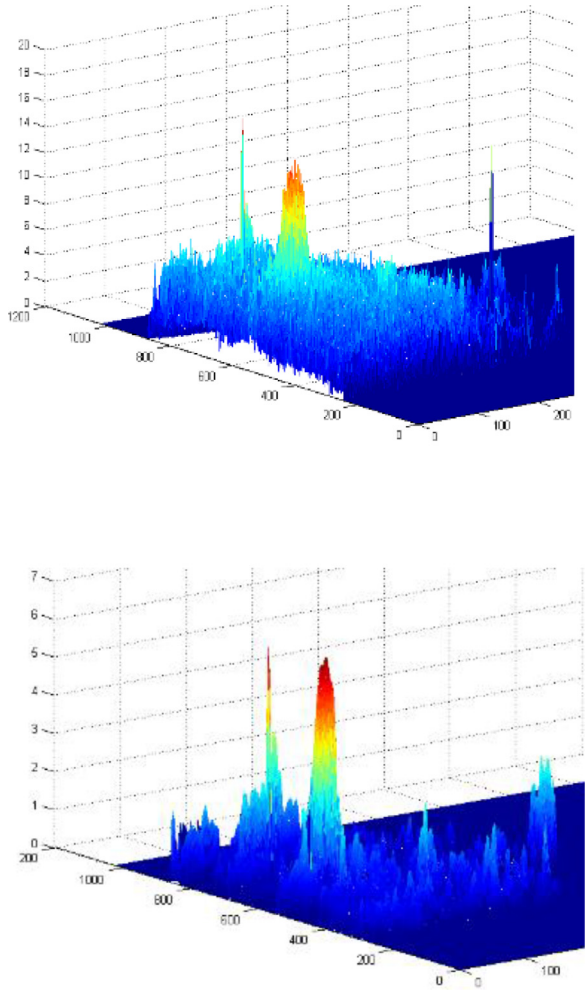

Fig. 1. A VBD map before (top) and after (bottom) the application of RICE.

1.2. Image enhancement methods

Several image enhancement methods for mammography have been published. As noted above, most such methods either manipulate the image histogram or apply a smoothing filter. To the best of our knowledge, none quantifies the content of dense tissue or a potential mass. In this section, we review several methods that have been developed for mammographic image improvement.

Early work (Sivaramakrishna et al., 2000) on enhancement methods include unsharp masking (Jong Kook Kim et al., 1997)(Lure et al., 1996), contrast-limited adaptive histogram equalization (Kim, 1997)(Pizer et al., 1987), region-based contrast enhancement (Morrow et al., 1992) and wavelet transformations (Laine et al., 1994). Most enhancement methods aim at better detectability of microcalcifications. In performance terms, there is a stark contrast between the approaches of enhancing mammographic regions that are potentially masses, and those for detecting calcifications. In most cases, the approaches designed for one type of enhancement, masses or microcalcifications, tend to smooth or ignore the other (Ji et al., 1994). Cheng et al. applied an entropy-based transformation to take an image into the Fuzzy domain to measure the local contrast and then enhance it (Bartella et al., 2006), similar approaches reported in other methods (Salmeri et al., 2008)(Lucht et al., 2000)(Ball & Bruce, 2007)(Bhateja et al., 2017)(Ball & Bruce, 2007)(Wu et al., 2013)(A. Jain et al., 2013)(Cheng & Xu, 2000). This, in essence, is very similar to adaptive contrast enhancement methods that stretch the contrasts of mammographic regions in a local context (Rangayyan et al., 1997). Wavelets can achieve similar results by a multi-scale frequency analysis approach, thus investigating individual components of a mammogram and highlighting the frequencies of interest (Tang et al., 2009). A different approach, inspired by the human visual system (HVS), reduces the need for a separate segmentation method. It uses the second derivative to highlight edge information by 2-tier image decomposition (Y. Zhou et al., 2010). Both the wavelet transform-based method and the HVS model do not work well in dense mammograms (such as BI-RADS D) where contrast is reduced and where ROIs do not have well-defined edges, thus lacking the high-frequency component. Filter-based approaches essentially regard image enhancement in mammography as denoising (Laine & Zong, 1996)(Matsuyama et al., 2013)(Gorgel et al., 2010)(Mencattini et al., 2008)(Romualdo et al., 2013)(Scharcanski & Jung, 2006)(Mencattini et al., 2008) (i.e. a proxy for better visualisation) from an "as-it-is" image. Such an approach does not take into account the breast thickness, tissue density, focal density and as a consequence *cancer masking*. Most such studies show that a significant difference exists in reviewer preference for images with masses and images with microcalcifications (Moradmand et al., 2012)(Sivaramakrishna et al., 2000).

The most common type of mammographic enhancement is based on probabilistic histogram equalisation (Pisano et al., 2000). More basic methods analyse the intensity distribution of the pixels across the image to determine the distribution on the spread. Such methods can work well on BI-RADS A and D, where the expected intensity distribution is often approximately uniform. However, they struggle with BI-RADS categories B and C where mammograms tend to have intensity distributions that are closer to bimodal. Adaptive histogram methods (for example CLAHE) address this issue by dividing the image into sections of variable intensities (Pisano et al., 2000). The method was originally designed for facial image enhancement, but its variants were later applied to mammography. Adaptive histogram equalisation methods do not preserve the brightness of the image. Brightness Preserving Bi-Histogram Equalisation (BBHE) aims to divide the image into two parts, based on the brightness levels. The method generates two images based on brightness thresholds and then apply adaptive equalisation to each separately. Subsequently, both parts are combined, which largely preserves brightness (Kim, 1997)(Chen & Ramli, 2003b)(Chen & Ramli, 2003a). However, it is not clear whether or not BBHE was effective in the case of craniocaudal (CC) view, as opposed to mediolateral oblique (MLO) views showed in the paper (Akila et al., 2015) where the bi-model intensity distributions are evident. In Recursive Mean-Separate Histogram Equalisation (RMSHE) (Chen & Ramli, 2003a), Chen et al separated the mean intensity of a mammogram to preserve the brightness of the two sub-images, following the essence of BBHE (Chen & Ramli, 2003b), but in a recursive fashion that aims to further enhance performance.

Image filtering and histogram equalisation methods were popular for use with digitised mammograms where noise removal, imaging artefacts and the pixel resolution of digitised mammograms were the main challenges. However, with the latest digital image acquisition scanners, the problems that these methods address have essentially been overcome. The new trends of mammographic image enhancement are based on the qualitative improvement of images in terms of their clinical value (i.e. visibility of cancers) as we explain in the following section, and not just a numerical metric for image enhancement (such as SNR, CNR, haziness, fractal dimension score etc.).

We have drawn a clear distinction between copious methods that enhance a mammogram by adapting to a histogram of intensities, as opposed to the localised, regional enhancement that is the basis for RICE. Though the use of histograms is widespread

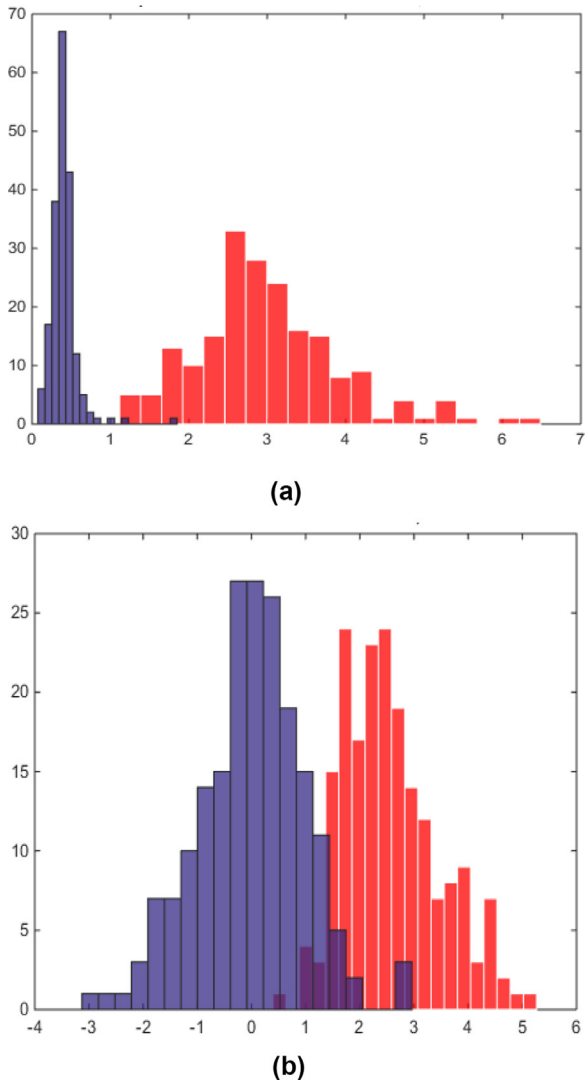

Fig. 2. a: Comparison of induced blurred (blue) vs un-blurred (red) regions in BI-RADS B. b: Comparison of induced blurred (blue) vs un-blurred (red) regions in BIRADS C.

throughout image analysis, a fundamental limitation of such methods is the following. Consider any image I (or region within an image) and create from it an image J by randomly scrambling the pixel values of I. Evidently, the two images I, J will not in general resemble in the least each other. However, their histograms are identical. This is the case whether I is a conventional mammogram image or a VBD density image like those in the paper. Though algorithms such as CLAHE have found widespread application, the interaction between global aspects of their behaviour (adaptive histogram equalisation) and the local aspect (contrast limited) often gives unpredictable results, as has been noted frequently in the image processing literature and which has led to a continuing stream of refinements to CLAHE.

There is a second point to make here. Contrast enhancement applied to mammography has to contend with varying composition of the breast (light adipose parenchyma resulting in haziness), or conversely varying response to blur in different BIRADS density categories. Fig. 2a and 2b show BIRADS B and C dense breast responding very differently to induced blurred. The effect is more aggressive on BIRADS B as compared to BRIADS C. This infers that the effect of applying low-pass filtering techniques and contrast stretching would affect these two categories very differently.

1.3. 'New' context of mammographic image enhancement

Over the past decade, due primarily to advances in the technology of digital mammographic scanners, assessment of mammographic image enhancement has advanced beyond sensitivity (taken for granted), towards specificity (how many cancers may be missed?). As a result, the context for use of enhancement methods has also changed. The risk of missing cancer (MISS-X) depends on several different factors, that we will summarise here but which are well explained in "20/20" (Ng & Lau, 2015):

MISS-1: The cancer is not visible because it is masked by dense tissue.

MISS-2: The cancer is not seen, possibly due to distraction by other dense tissue.

MISS-3: The cancer is seen, but it is interpreted wrongly due to overlapping tissues.

MISS-4: The cancer is not present in the image.

MISS-5: Cancer is present, but not visibly discernible.

With a few exceptions (Mainprize et al., 2016)(Mainprize et al., 2018)(Hinton et al., 2016)(Aghaei et al., 2017), there appears to be a limited understanding of focal density and masking in the mammographic image analysis literature. Our method aims to reduce MISS-1 and MISS-2, though, because of the overall improved contrast and highlighted focal densities, we are confident that it helps reduce MISS-3. MISS-4 is not an image processing issue; nevertheless, good positioning measures will improve it (Peart, 2014)(Popli et al., 2014). For MISS-5, image enhancement followed by more informed machine learning approaches may usefully be combined (Le et al., 2019). comprises iterative neighbourhood estimation, subtraction, and merging that subtracts the encompassing tissue surrounding focally dense regions. At the same time, RICE detects and iteratively suppresses normal parenchyma. In theory, if a density map does not contain any dense regions, the breast region in the contrast-enhanced image should be almost 'blank'. RICE is particularly effective on volumetric density maps generated by an increasing number of commercially-available methods, for example, Quantra (Volumetric & Software, 2010; Wang et al., 2012); Volpara (F. Janan et al., 2014; Teo et al., 2016); and Densitas (Abdolell et al., 2017). These provide either estimation of tissue density or an approximation to x-ray attenuation absorbed at each point of a mammographic image, and this helps not only to detect but also to quantify and further standardise focal density scores. Note that there does not currently exist a clinical standard against which to quantify a focal asymmetry or a focal density. Lacking such a standard, which inevitably limits validation, we have resorted to the output of software for density estimation, primarily because it is a physical measurement of breast tissue, and in part, because numerous papers have shown a link to breast cancer detectability and risk. More specifically, we have used VBD maps because it is multi-vendor, widely available (and available to us), has been used in hundreds of studies of breast density, because of its positive impact in assessing breast cancer risk using volumetric mammographic density, and on the performance of breast cancer screening program using full-field digital mammography (Chiu et al., 2010). We stress, however, that RICE can be applied straightforwardly to DICOM regular mammographic images. We implement RICE in 5 steps.

1.4. Segmentation

First, we segment the breast region (beneath the skin-line) into smaller regions that share a similar texture and density. Consider the volumetric density map as a surface plot $V(x)$, that has a high-frequency element corresponding both to stromal tissue and noise. Since we are interested in the ROI as a whole and not the added high-frequency component, we approximate $V(\bar{x})$ locally over

smaller regions. There are several ways to do low-level descriptive segmentation (Srinath, 1992)(Vala & Baxi, 2013)(Morar et al., 2012)(Therrian, 1981)(C. Zhou & Chan, 2001)(A. K. Jain & Farrokhnia, 1991)(Li et al., 1997)(Hong & Brady, 2003)(Faraz Janan & Brady, 2015). In our current implementation, we have elected to use a method that works well in practice, is robust, and efficient (Achanta et al., 2010). We use Simple Linear Iterative Cluttering (SLIC) to provide a piecewise constant approximation to the surface locally in the form of small texture bound patches called 'superpixels'. This may be replaced by alternative segmentation methods that are able to segment the entire breast region. A pipeline method that also uses SLIC segmentation for mammographic image enhancement is given in (Chu et al., 2015). We note that all segmentation algorithms, whether based on computer vision methods or low-level image processing techniques, often result in over or under-segmentation. This is especially the case in the presence of extensive "texture" in the form of curvilinear ductal/stromal structures such as in BI-RADS C. The RICE multi-scale iterative routine tackles over-segmentation by combining small facets belonging to the same region. It also deals well with under-segmentation by breaking down larger regions into smaller superpixels. Each segmented region $\{R_i S\}_{i=1\ldots n}$ is identified separately for further processing.

1.5. Constant estimation of breast regions

The second step is to compute the mean value for each segmented region and generate segmentation masks. For a segmented mammographic map $V(\bar{x})$, where the maximum size of a patch is specified as a prior, we generate a mean density map of superpixels $S(\bar{x})$ as shown in Fig. 3(b). The goal is to create an output map $L(\bar{x})$ in which ROIs are locally enhanced, whereas those of lesser clinical interest is suppressed. This embodies the fact that breast density, as computed in VBD, is a physiological parameter that reflects the breast tissue composition, as opposed to a brightness value in which tissue composition, exposure time, tube voltage, etc are confounded. In Fig. 3(c) we show how the piecewise constant approximation of segmented regions using its mean value correspond to the VBD map.

We note that the size of the abnormality does not significantly impact the performance, due to the iterative nature of the algorithm (see below). For instance, an abnormality that is over segmented in one SLIC iteration would be re-combined in together in the following iteration, as described in Section 2.1.

1.6. Of local neighbourhood

The third step is to estimate the density of the tissue surrounding each region. Suppose that each smaller region R_i is associated with a constant mean value of the ith region. Then the segmented region $S(\bar{x})$ results from binarising and dilating using a circular Integral Invariant (II) (Manay et al., 2006) to capture the neighbouring tissue. We refer to (Faraz Janan et al., 2015; Faraz Janan & Brady, 2013) for a detailed explanation of how II may be adapted as an information handler for neighbouring tissue. II adapts according to the shape and size of an ROI, an expedient that could be used in several ways beyond the purview of this work. II provides an extended region R_i^+ which includes the ROI R_i and its immediate surroundings. The mask of the immediate surroundings is:

$$N(R_i) = R_i^+ - R_i \tag{1}$$

The mean density of the neighbourhood is μ_i^N, for the R_i by μ_i^0 where N stands for the neighbourhood and 0 stands for the region in question. Volumetric density V_{R_i} (in mm^3) for each R_i is given by:

$$V_{R_i} = \delta_i^O\left(x,\ y,\ \dot{d}\right) dx\, dy\, d\dot{d} \tag{2}$$

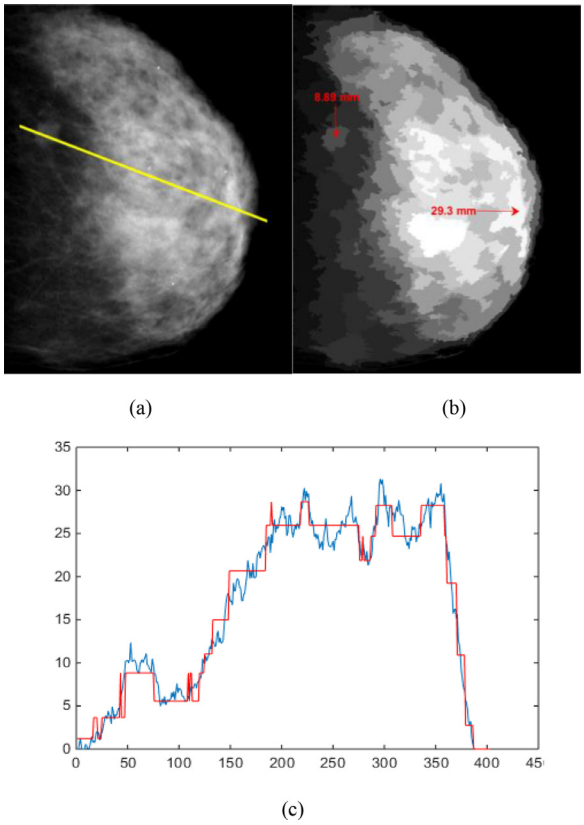

Fig. 3. (a) A VBD map; (b) Piecewise constant approximation of SLIC segmented regions using mean values, $(\bar{x})$. Using red arrows we highlight the mean density of two example regions; (c) the correspondence between the pixel density values in (a) and (b) extracted along the yellow line in the VBD map.

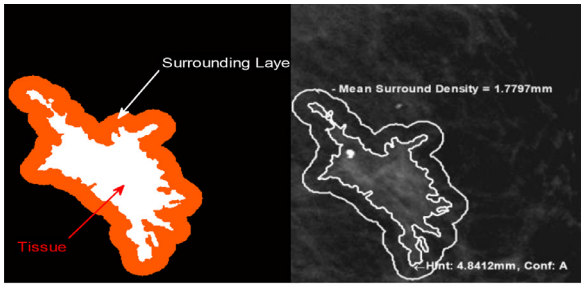

Fig. 4. (a) The combined mask R_i^+ of a segmented region R_i along with II diffused region highlighting immediate neighbourhood or the surrounding tissue in the orange colour $N(R_i)$; (b) Mean thickness of the tissue μ and its neighbourhood μ_i^N.

Where $\dot{d}$ is the density of $V|_{\delta_i^O}$ at $\{(x_j,\ y_j) : j \in R_i\}_{j=1\ldots M}$. $x_j,\ y_j$ are the spatial coordinates for the segmentation mask. We refer the reader to Fig. 4 for a schematic explanation. δ_i^O is the surface volume of a region in a given density map.

1.7. A local contrast map

The fourth step is to compute a local contrast map L($\bar{x}$) at all points around the boundary of a segmented region R_i such that the ROI is enhanced. This is a subtraction process that imposes the following two conditions:

1) For any R_i, if the mean of the background tissue has greater density than the region itself, then it is considered to be normal

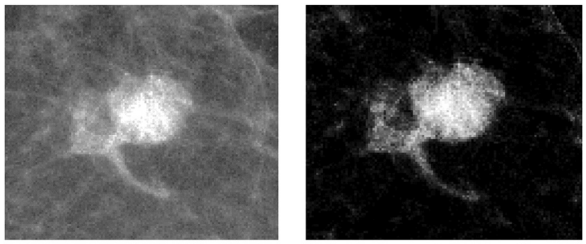

Fig. 5. (a) A mass with connected components (b) Visibility and the margins of the mass significantly improved after applying RICE.

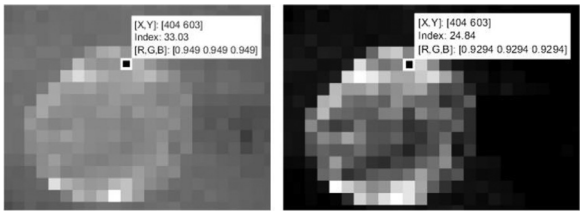

Fig. 6. A small circular region around 7 pixels in diameter before (left) and after (right) the application of RICE. The index specifies the density of the pixel in Volpara density maps.

tissue. In this case, subtract the mean μ_i^O of the region from each pixel in the region.

2) For any,R_i if the background has a lower density than the region; then the mean of the background μ_i^N is subtracted from each pixel in the region. An offset is added for pixels resulting in negative numbers.

$$L(\bar{x}_i) = \begin{cases} V_{R_i} - \mu_i^N \Leftrightarrow \mu_i^N > \mu_i^O \\ V_{R_i} - \mu_i^O \Leftrightarrow \mu_i^N \leq \mu_i^O \end{cases}, \; i = 1 \ldots n \tag{3}$$

Recalling Fig. 4, the segmented region has a mean density of 4.8mm^3, whereas that of the surrounding region is 1.7mm3. After the first iteration of RICE, the resulting mean thickness of the region is: 4.8 – 1.7 = 3.1mm^3. There is a high-density difference between the thickness of the tissue and its surrounding, thus indicating a focal density (labelled as Conf. A in the figure). Fig. 5 shows another example where the appearance of a confirmed mass is enhanced after all of the iterations of RICE. The example shows how RICE can effectively suppress normal parenchyma while preserving the ROI. Fig. 6 shows a calcification (7 pixels in diameter), embedded in a dense background with poor contrast, enhanced using RICE. A small regions of sufficiently high contrast are both picked up and amplified both by SLIC and by the iterations of RICE. A simple example of that is shown earlier in Fig. 1a, where a microcalcificiation is a small region that stands out above the surrounding noise floor. Note that this is in part a consequence of us working with VBD (and similar) density images: VBD makes the assumption that tissue is either “dense” (“interesting” in VBD speak) or “fat”; however, the attenuation of a microcalcification is substantially greater – generally reckoned to be 20-30 times – that of “interesting tissue” (see (Highnam & Brady, 1999)), and so microcalcifications appear much “higher” than their cross-section diameter in a VBD image. Fig. 1b shows that the thin, high region is preserved through the iterations of RICE. In Fig. 6 we show another example of a relatively small region in a poor contrast region enhanced considerably.

Fig. 7 shows a region and its surroundings, together with the corresponding density histograms. While the segmented region in (a) has a normal density spread; the surrounding region in (b) has a two-peak distribution. A scrap-mark is an extended line resembling an edge resulting from the non-uniform intensity/density distribution of the neighbouring tissue. This could affect the apparent structure of the breast anatomy inducing unwanted new information. The background suppression process may result in an artefact which we call the ‘scrap-mark effect’. Fig. 8 shows a typical example of a scrap-mark artefact. In the image, the effect is obvious in the form of a dark edge passing vertically close by the mass towards its right side. The figure shows two density profiles extracted on a normalised scale from the original image and the processed image after the first RICE iteration. From the graph, it can be seen that the contrast of the ROI has been significantly enhanced in the RICE processed image. However, an unwanted artefact in the form of a small peak has emerged. This effect is mitigated using an iterative mechanism, explained in the late r section.

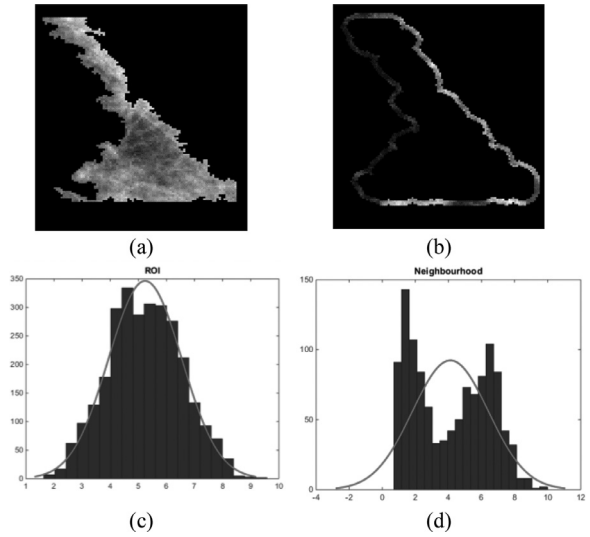

Fig. 7. (a) a segmented region; (b) neighbourhood of the region in (a); (c) normal density distribution of the region (a); (d) two-peak density distribution of the neighbourhood (b).

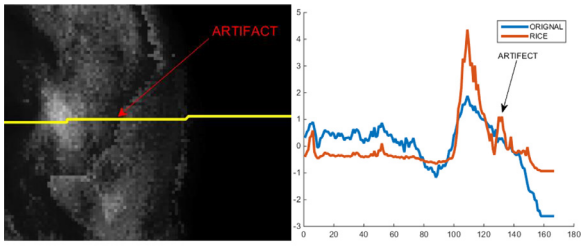

Fig. 8. (a) The scrap-mark artefact towards the right of an ROI; (b) the density profile extracted along the yellow line for RICE processed and the original image on a normalised scale.

1.8. Suppression

Finally, steps 1-4 are performed iteratively at multiple scales of II diffusion. These steps are formulated into a tail-recursion model derived in the next section (i.e. The Iterative RICE Model), which is explained briefly here for completeness. In the RICE model Step-1, 2 and 4 remains the same. However, in Step-3 we begin with small scales of II diffusion to capture the immediate neighbours, gradually progressing to larger scales. This iterative mechanism corrects any under- and over-segmentation, as well as preserving the edge shapes and subtle details of dense regions (i.e. ‘interesting tissue’).

Relatively small scales of ROI diffusion define the shape of a region, thereby capturing fine details. Larger scales deal with the

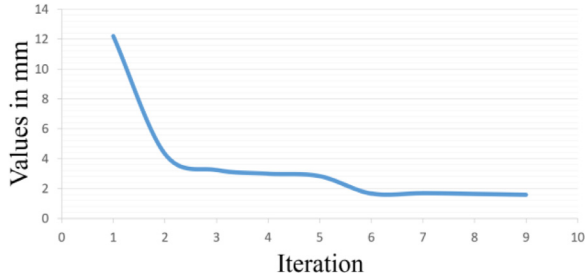

Fig. 9. Reduction in tissue density for a mass in Fig 9 over iterations.

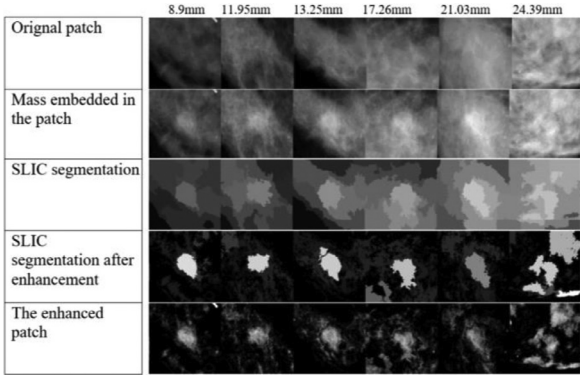

Fig. 10. Normal tissue suppression over several SLIC iterations.

coarse level information by helping the normal parenchymal suppression, overcoming the scrap-mark effect and helping to merge superpixels belonging to the same region.

Fig. 9 shows that the mean density of a mass gets closer to the ground truth reduced over 4 iterations. Moreover, by using the 'Elbow method' (Kodinariya & Makwana, 2013) borrowed from data clustering application, we find that 4 iterations effectively suppress the normal parenchyma while maintaining the shape of a given spicular region. This assumption is supported by our results from Fig. 15 in the results section. In the Fig. 10, we illustrate an example of the embedding process, followed by the enhancement using our method. The row with SLIC segmentation (before and after enhancement) illustrates the effectiveness of our method. The last column is composed of an extremely dense patch; hence difficult to differentiate between the mass and dense areas within the patch.

After the completion of each iteration, we combine residue maps $L(\bar{x}_j)$ from the current and earlier iterations along with a weighted version of the VBD map. The output of the complete process is called the 'RICE map'. The summation of VDB/mammogram in the averaging process helps to capture the full entropy information in a given mammographic image, where even the slightest details are retained. However, the iterative subtraction and averaging enforce a weighting scheme that benefits focal densities and penalises the uninteresting normal parenchyma. The essence of the recursive process is those focal densities persist over multi-scale iterations to become more visible with an increased contrast to the background. A fuller description of the RICE model and its mathematical derivation is given in the next section.

2. Iterative model

The iterative model is the core of RICE. It recursively combines images that have been enhanced in previous iterations with a weighted sum of the original image at multiple scales of diffusion. For each iteration, the output image is comprised of three elements: 1) the newly processed RICE image; 2) enhanced images from previous iterations; 3) the original image that is weighted by a decreasing exponential value β. The input image for each iteration is the output of the previous iteration. After the final iteration, each pixel is subjected to a majority voting for corresponding pixels through the enhanced images produced during every single iteration. For any mammographic image I (either the VBD map V(x) used earlier, or an intensity-based image, or synthetic mammograms) the enhanced image I_{RICE} is generated by the following process over n iterations.

2.1. Iteration 1

We suppress the background tissue to attain the residue map r_1, as explained in steps 1-4 above.

$$I \rightarrow r_1 \tag{4}$$

I. Rescale r_1 with $\propto_1$, such that

$$\max(r_1) \rightarrow \max(I)$$

$$\min(I) = \min(r_1) = 0 \tag{5}$$

II. From these constraints, we determine α_1 as:

$$\propto_1 = \frac{\max(I)}{\max(r_1) + 0.0001} \tag{6}$$

III. We then generate the enhanced map e_1

$$e_1 = \beta\ (I + \propto_1 r_1),\ \ for\ \beta = 0.5 \tag{7}$$

The scaling factor β is a tuning parameter that may be adjusted according to the type of mammographic imaging modality used to generate the RICE maps. We have found that a value of $\beta = 0.5$ works well for VBD maps. However, this value can be adjusted if the method is applied to intensity images or synthetic mammograms generated from DBT stacks (for instance, Hologic C-View (Greer, 2014)).

2.2. Iteration 2

The same process is repeated to generate the enhanced map e_2 after the second iteration from the residue map r_1, scaled by $\propto_2$, which is:

$$e_2 = \beta^2 I + \beta^2 \propto_1 r_1 + \beta \propto_2 r_2 \tag{8}$$

$$\text{Where},\ \propto_2 = \frac{\max(e_1)}{\max(r_2) + 0.0001} \tag{9}$$

r_2 denotes the new residue map after the second iteration. We derive e_2 as follows:

$$\begin{aligned} e_2 &= \beta(e_1 + \alpha_2 r_2) \\ &= \beta(\beta(I + \alpha_1 r_1) + \alpha_2 r_2) \\ &= \beta^2 I + \beta^2 \alpha_1 r_1 + \beta \alpha_2 r_2 \end{aligned} \tag{11}$$

2.3. Iteration 3

This is repeated, for example:

$$e_3 = \beta^3 I + \beta^3 \propto_1 r_1 + \beta^2 \propto_2 r_2 + \beta \propto_3 r_3 \tag{12}$$

2.4. Iteration n

$$e_n = \beta^n I + \beta^n \propto_1 r_1 + \ldots + \beta \propto_n r_n \tag{13}$$

$$e_n = \beta^n I + \sum_{i=1}^{n} \beta^{n-i+1} \propto_i r_i$$

From this, it is possible to estimate the amount of breast parenchyma that has been suppressed from the original image, and in theory to recover a reasonable estimate of the original image.

2.5. Scale-space analysis

Since $0 < \beta < 1$ it follows that $\beta \to 0$ rapidly, therefore we may approximate $\forall n > m, \beta^n = 0$.

$$mean\{e_n\} = \frac{1}{m}\sum_{i=1}^{m} e_i = \frac{1}{m}\sum_{i=1}^{m}\beta^i I + \sum_{i=1}^{m}\beta^{i+1}\alpha, r \tag{14}$$

Consider the first term:

$$\left(\frac{1}{m}\sum_{i=1}^{m}\beta^i\right)I = \left(\frac{1}{m}\left(\frac{1-\beta^{m-1}}{1-\beta} - 1\right)\right)$$

$$I = \left(\frac{1}{m}\left(\frac{\beta}{1-\beta}\left(1-\beta^{m-1}\right)\right)\right)I \tag{15}$$

Since we set $\beta = \frac{1}{2}, \beta = (1-\beta)$. Hence the term essentially equals $\frac{1}{m}I$. We now derive the second term. We can re-group the terms by $\alpha_j r_j$. This can be written as:

$$\alpha_1 r_1 \sum_{i-1}^{m}\beta^i + \alpha_2 r_2 \sum_{i-2}^{m}\beta^i + \alpha_3 r_3 \sum_{i-3}^{m}\beta^i + \ldots$$
$$\left(\sum_{i=1}^{m}\beta^i\right)\left(\alpha_1 r_1 + \alpha_2 r_2(1-\beta) + \alpha_3 r_3\left(1-\beta-\beta^2\right)\right) \tag{16}$$

Assuming that the term $\sum_{i=1}^{m}\beta^i \approx\sim 1$ shows that the second term is a weighted sum of the terms $\alpha_1 r_i$ in the ratios 1:1/2:1/4:1/8..1/n.

This illustrates that for a sufficient number of spatial scales of SLIC, almost none of the entropy information from within a mammogram is lost, while at the same time it successfully suppresses the local parenchyma and estimates focal densities. The focally dense regions that persisted over multiple scales are enhanced, whereas the normal parenchyma is effectively suppressed (not entirely removed).

2.6. The final step

Finally, to generate the output, I_{RICE}, we apply a function $\emptyset$, which could be majority vote (or mean, median) for each pixel through every e_i. The majority voting process mitigates the scrapmark effect.

$$I_{RICE} = \emptyset\left(\lim_{i=1\to n} e_i\right) \tag{17}$$

2.7. SLIC regularisation

Note that this step is only relevant if SLIC is used to segment regions in the RICE model. SLIC's regularisation coefficient δ controls how regular (hexagon) or deformable the shape of a superpixel should be used (Vedaldi & Fulkerson, 2010). SLIC uses this as a seed value to form clusters of similar pixels. In practice, it suffers from over-segmentation when applied to images with complex spatial and textural regional differentiation. This has a direct impact on the estimation of the local neighbourhood of segmented regions, especially in the first two iterations where most of the 'normal' parenchyma is suppressed. If δ is estimated sensibly, this not only reduces the number of RICE iterations to produce good results but also preserves the borders of the ROI more effectively. For the first iteration, we use the median of the original image, $\delta_1 = \tilde{I}$, whereas for the remaining iterations we use the median value of the output images from the previous iterations. This enables us to set up an automatic balance between the deformability of a superpixel and its size.

$$\delta_i = \widetilde{e_{i-1}} \tag{18}$$

applied RICE to VBD maps obtained from the 'Manchester 50/50 dataset' (a subset of the PROCAS study samples (Astley et al., 2018)(Sergeant et al., 2012) provided as part of the ASSURE project). The set of cases (VBD maps) includes 50 screen-detected cancers and an equal number of controls, all anonymized, and all with bilateral CC and MLO views. They were all imaged using a clinical GE Senograph Essential. The mammograms were converted to VBD maps using the Volpara Research Platform 1.0. In an observer study, all focal densities (cancer or non-cancer) were enhanced as expected. More precisely, all the dense regions were correctly identified; but with a high false positive rate. To reduce the number of false positives, an in-house mass detection algorithm (F. Janan et al., 2014) was applied to detect the masses in the mammograms. We stress that the objective of RICE is ***not*** mass detection per se, rather mammographic image enhancement, which may aid CADe, and on which it performed well. In the results shown below, masses were correctly detected and segmented in 46 mammograms using (F. Janan et al., 2014); however, in 4 images (2 dense, 1 fatty and 1 moderately textured) masses could not be identified either visually or by a locally deployed computer-aided detection (CADe) system. Evidently, a state-of-the-art system for detecting/proposing soft tissue masses (e.g. from ScreenPoint Medical or iCAD) could replace this step.

Qualitatively, contrast enhancement of dense regions is not achieved at the expense of tumours in fatty regions of the same breast. To be visible on a mammogram, a typical tumour has a higher density than the surrounding tissue. Fig. 11 shows an example of a low-density neighbourhood in an otherwise BI-RADS D breast. The tumour is situated close to the chest-wall, away from the breast peripheral region (red arrow). The central region is uniformly dense (it is BI-RADS D) and is reported to be normal tissue. Volpara density maps suggest that the breast inner region around the centre, which is normal dense tissue, is far denser than the mass (refer to Fig. 3 for actual density values). As can be seen, in this case, RICE effectively suppresses the dense tissue while enhancing the visibility of the tumour. We re-emphasise that RICE enhances the ROI; it does not classify the enhanced region as a mass.

A fundamental limitation of density estimation using RICE, or any other method that relies on 2D mammographic modalities, is the impact of breast thickness on tissue density. Breast have variable thickness when compressed in a mammography machine. To find the density of an ROI, we subtract the density of the neighbouring tissue from it. We base this on the assumption that the density of normal tissue above and below the ROI is approximately the same as that of the immediate neighbourhood. Based on this assumption, while estimating the ROI density and subtracting the neighbourhood, we also subtract an equal amount of normal tissue that substitutes the ROI in the neighbourhood–thus the density estimate of ROI should be lower than that of the actual tissue. Fig. 12 is a sketch of the process. This has minimal effect on fatty and moderately dense breast. However, it could affect ROI density estimation in a very dense breast by subtracting too much of the surrounding tissue. A means to include breast thickness into the model, for example, formulating a certain ratio that could reflect upon the thickness of the ROI and the breast, could compensate for this effect. Our method accurately detects focal densities in highly dense breast.

To test RICE in unmasking tumours in a dense breast, we extracted a clinically confirmed mass and embedded it into four types VBD maps categorised as Volpara Density Grades (VGD). The VDG score strongly correlates with the actual BI-RADS classification (Lee et al., 2015)). Furthermore, this experiment tests the performance of RICE in identifying and suppressing the normal parenchyma surrounding the ROI in all density classes. The experiment is as follows:

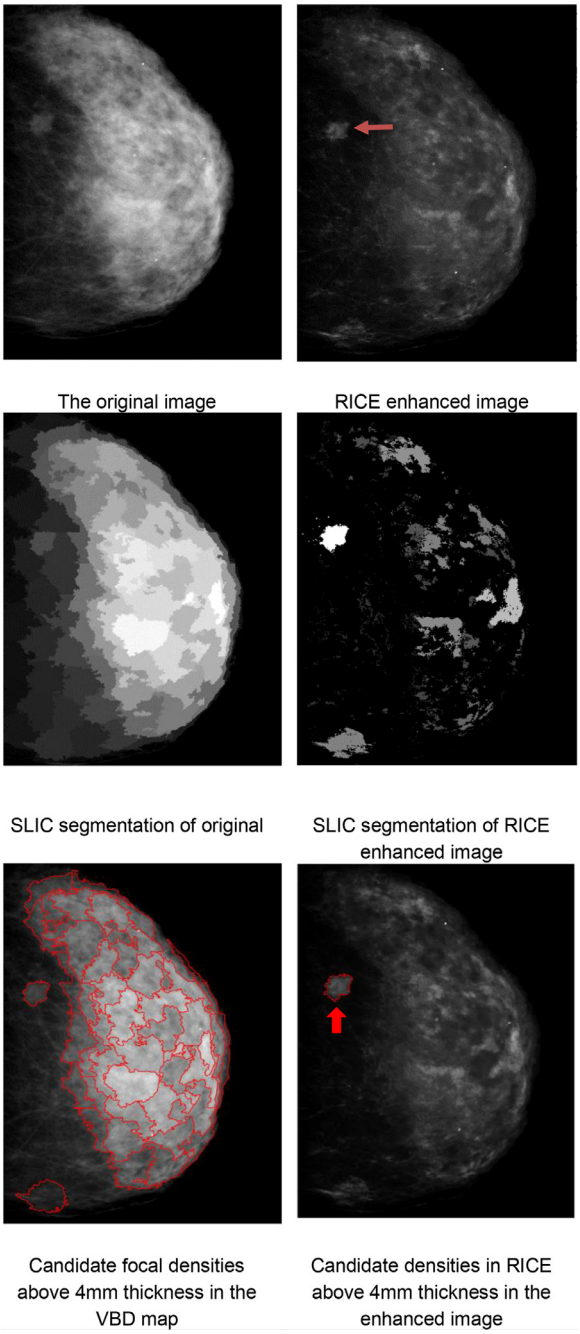

Fig. 11. The density map is enhanced by suppressing normal dense parenchyma while enhancing the visibility of tumour in a lighter background (highlighted with a red arrow).

1 First, embed a mass into various VBD maps labelled by their VDG scores.
2 Apply RICE to suppress the normal parenchyma and quantify the density of the embedded mass in the enhanced mammogram.
3 Assess the consistency in the density of the mass in enhanced RICE maps throughout all VDG categories.

Several factors could impact the consistency of the mass density in the enhanced RICE maps. These include: the density and texture of the host breast on the shape of the segmented region; the thickness of the host mammogram; the non-biological basis of the embedding procedure and so on will affect the density of the mass in enhanced RICE images. As the volumetric density for breast

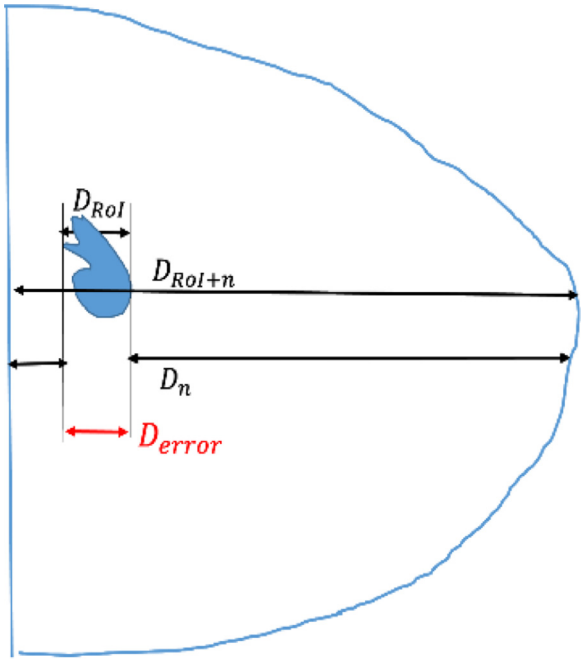

Fig. 12. A demonstration of density estimation error.

parenchyma across the BI-RADS categories could vary by an order of magnitude, we expect the density of the mass in the enhanced images to show little variation across categories, and to be within an acceptable margin of error. Fig. 14 shows the results of inserting a known mass into 24 VBD maps (6 from each VDG categories). After the fourth iteration, the density of the mass is consistent across all four categories with a mean mass density of 3.18mm^3 (against the ground truth 3.96mm^3), variance 0.75mm^3 and the standard deviation of 0.87mm^3. Fig. 15 shows the density of the inserted mass after 4 RICE iterations in all VDG categories. This is the mean density value of the mass extracted from 6 VBD maps per category. From Fig. 14 and Fig. 15 we conclude that RICE produces consistent results for suppressing normal parenchyma and in estimating the volumetric density of an ROI in all breast density classes. It implies that were we to embed a mass into a dense mammogram/VBD; RICE would unmask and estimate density effectively, thus sharply reducing the risks of MISS 1-3.

Although in this paper we focus on the application of RICE to mammographic images, nevertheless, our experiments suggest that RICE can be applied beyond mammography. Fig. 16 shows a scanning artefact where a metallic circuit is imaged in the mammogram. RICE significantly improves the contrast and visibility of the circuit. We also applied RICE on other mammographic modalities, in particular, unprocessed DICOM mammograms (normal intensity maps); synthetic mammograms generated from reconstructed stacks of DBT scans (similar to C-View (Greer, 2014)); and SAR images (Tromans et al., 2012).

As above, there is no notion of quantitative volumetric breast density in the images produced by any of these modalities. Despite that, we have found consistent and significant improvement in the visibility of dense parenchyma in these images. Fig. 17 shows a few examples where RICE enhances the contrast and improves the visibility of dense regions in routine mammograms. Fig. 18 shows RICE applied to synthetic mammograms; and in Fig. 19 RICE is applied to SAR images (C. Tromans et al., 2012; C. E. Tromans et al., 2012).

An important question the reader may ask is, how well does RICE perform with respect to the abnormality size? There are two aspects to consider: size; and density. The former might be expected to impact, for example, on the SLIC step Section 2.1). The

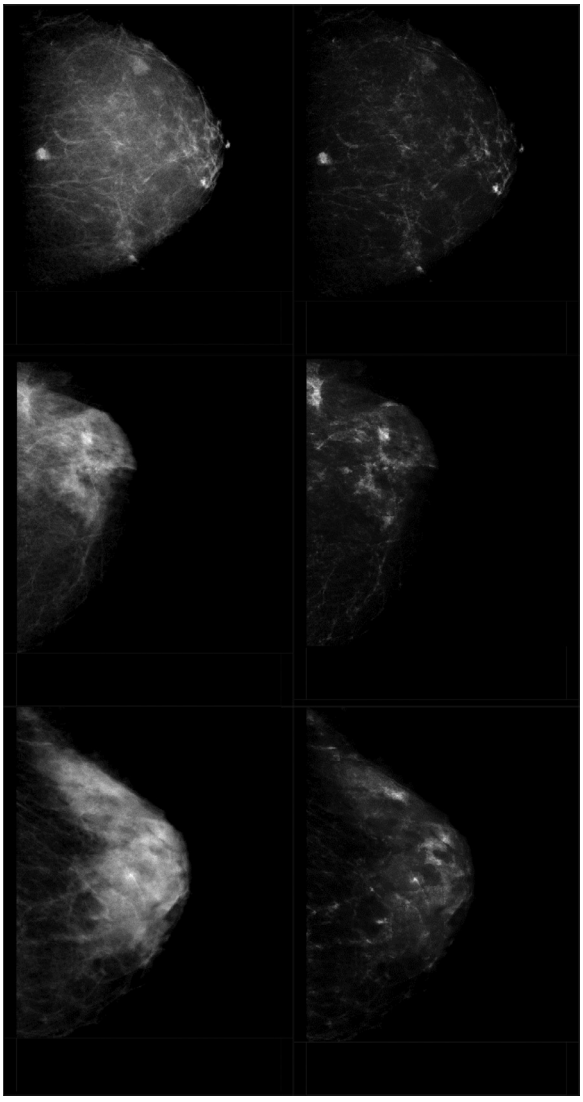

Fig. 13. Examples of RICE enhanced Volpara density maps.

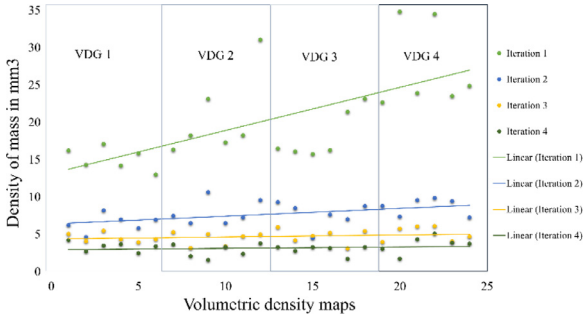

Fig. 14. Estimated density of a mass inserted in 24 VBD maps (6 from each VDG category) after several iterations of RICE. It can be seen hat the density of the mass is consistent after the fourth iteration across all VDG categories.

latter impacts, *inter alia*, local contrast, and so may impact detection. Evidently, an abnormality of size (say) 1 pixel, and with minimal contrast to dense surroundings, would be treated as noise and would not be enhanced. For the density, the recursive nature of RICE ensures that a sufficiently dense region is maintained, even if it is small, such as a microcalcification (Fig. 1 and Fig. 6). Consider the case where both the size and the contrast of (say) an

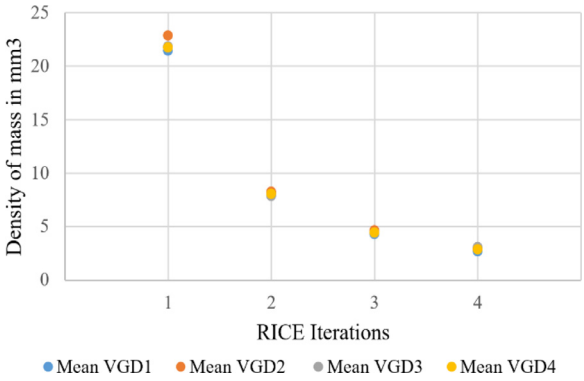

Fig. 15. The mean density of the mass for VBD maps from each VDG category through four iterations of RICE.

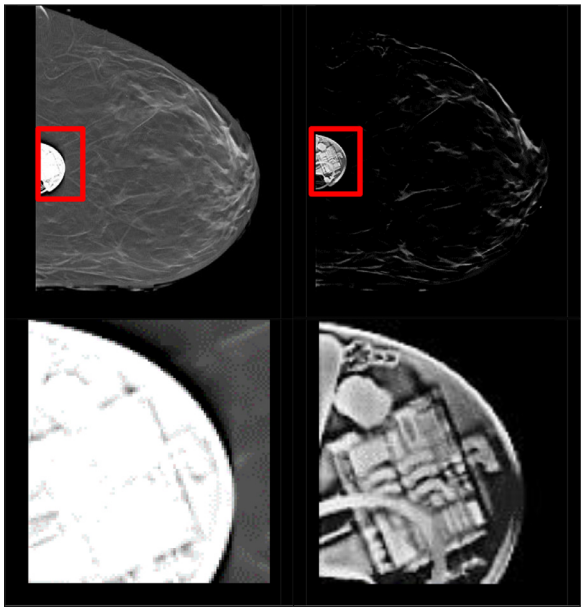

Fig. 16. RICE improving the contrast and the visibility of a non-mammographic texture.

implanted region are reduced. At a certain point, as the contrast of the implanted region and the neighbourhood reduces, the region would no longer be picked up in Step 1 (Section 2.1, SLIC). There is nothing RICE can do in such a case. However, when a region is picked up by SLIC as a candidate ROI, would RICE suppress it? This is addressed in Sections 2.3, 2.4 and, more importantly, in Section 3, which is the core of RICE. Here the key parameters are α_1, β. The first of these is defined in Equation (5), while the latter is set to a value of 0.5 for VBD depth maps (Equation 7). The subsequent analysis in Equation (13) and the Scale Space analysis (Equations 14, (15) show that a region, of sufficient size to be picked up in SLIC or sufficient contrast but small size will be preserved in RICE. We include a further example (Fig. 20) with intermediate steps to show that RICE does not smooth the margins of a malignant mass.

To confirm that the enhancement process suppresses what we consider is normal parenchyma encompassing a region of interest, we test the consistency of our method using a matric we call tissue to background ratio (TBR). We compare ROIs in post RICE regions for Volpara and SAR, both of which are quantitative images and provide an approximation of mammographic density per pixel. Please refer back to Fig. 4 in section 2.3 to see how TBR is computed. In Fig. 21 we can see that TBR for both Volpara and SAR images is very similar, despite the composition of these images

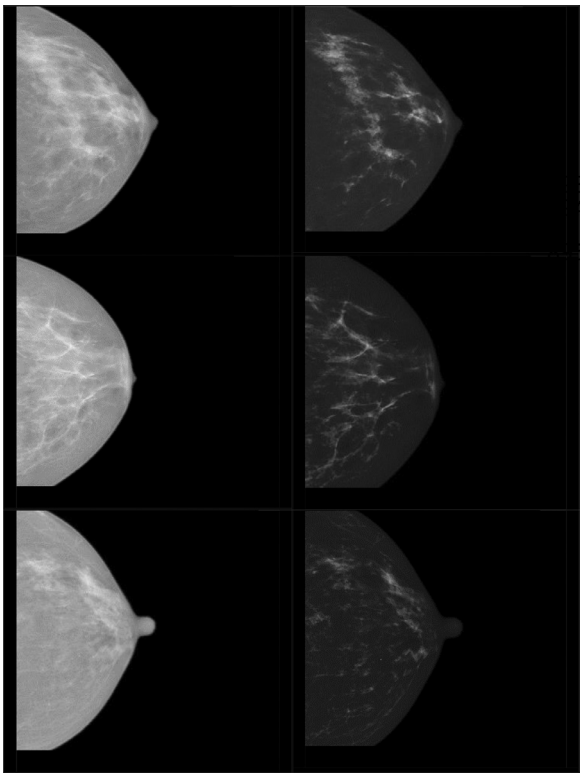

Fig. 17. RICE applied to intensity based mammograms(DICOM x-ray images).

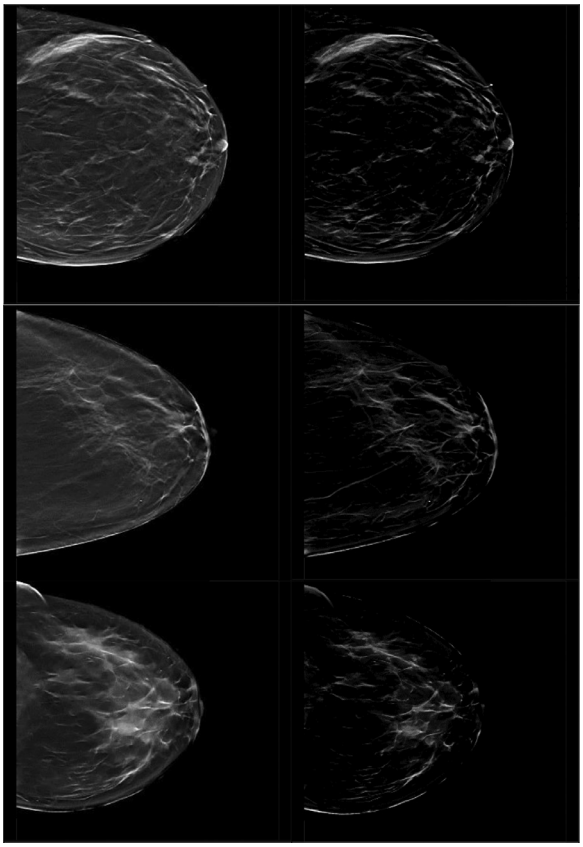

Fig. 18. Synesthetic mammograms generated from DBT (left), enhanced using RICE (right).

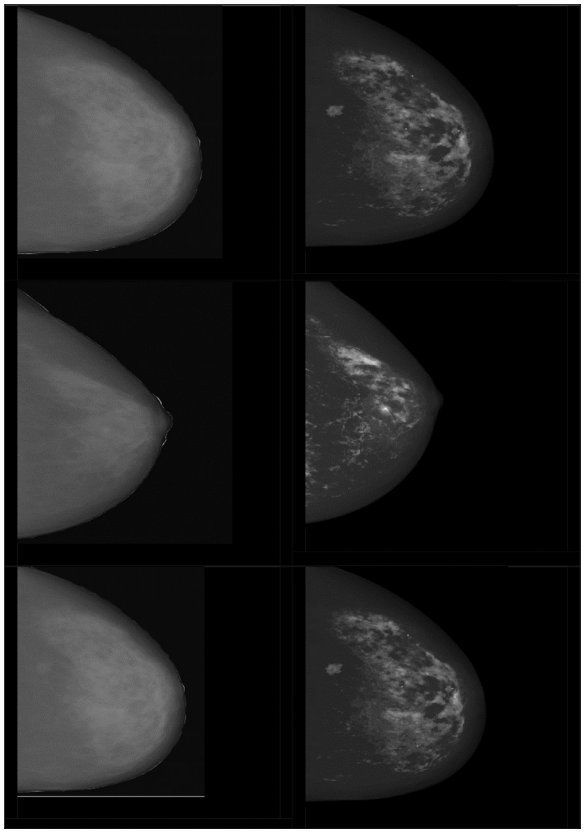

Fig. 19. SAR images (left), enhanced using RICE (right).

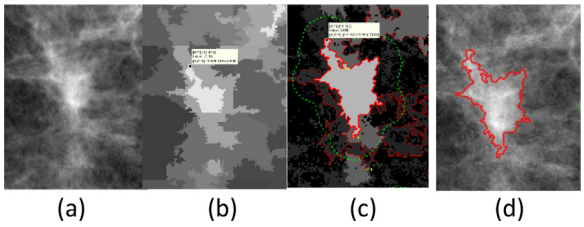

Fig. 20. Effect of RICE on tumor margins. (a) A tumor patch; (b) Piece-wise constant estimation after the first RICE iteration; (c) Red is the boundary drawn using an inhouse method (Janan et al., 2014), green is the ground truth; (d) The segmentation boundary overlaid on the original image.

and the methods used to compute density are very different - uses distinct physics models to estimate independent x-ray attenuation absorbed per pixel. In Fig. 22 we further evaluate the consistency for 15 masses and find that the TBR scores closely agree with each other.

Next, our method enables us to compute a single focal density score for the whole breast by aggregating densities of the tissue remaining after enhancement by our method in each breast quadrant. Fig. 23 (a) and (b) shows a bilateral pair, that masks an 18mm grade 5 invasive ductal carcinoma detected in the right breast from a 'prior' exam. The breast is extremely dense and was classified as BIRADS D, having 30.2% of mean volumetric breast density and a Volpara VDG grade 4. This is an interval cancer and perhaps 'should have been detected' when the densities in the right breast began inexorably to rise. We analyse this clinical case using RICE to quantify focal densities in the four classical breast quadrants to assess the change in densities over time. As usual, we automatically: detect the breast boundary; find the nipple; identify the skin-line (buffer between the skin and the breast region); and divide the breast region into 4 quadrants based on taking the nipple as a ref-

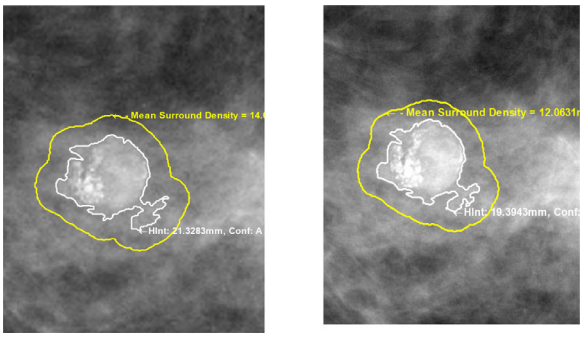

Fig. 21. Comparison of TBR of 0.68 for Volpara (left), and 0.62 for SAR (right).

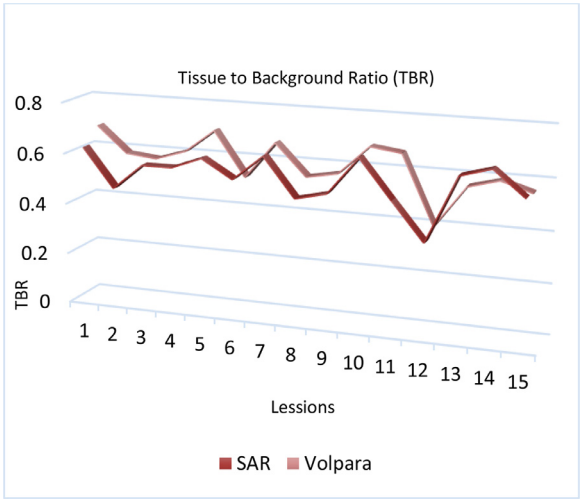

Fig. 22. TBR scores for 15 lesions, Volpara vs SAR, showing that our method consistently suppresses the normal tissue surrounding ROIs.

erence. Fig. 23 (c) and (d) shows that the right (infected) breast has a higher focal density (FD) score than the left (5.16 vs 6.86), thus confirming the laterality of cancer.

Fig. 24 shows a pattern of change in focal densities for the left breast over time. Moreover, what is unclear in the clinical report, but is clear from the FD analysis after applying our method, is that quadrants Q1 and Q4 are accumulating asymmetries in the right breast years before cancer appears. This suggests that there is a potential for FD measure to predict the likelihood of a developing abnormality related to the asymmetrical accumulation of densities in the breast over time. is an image enhancement method, that has been developed primarily for mammography and applied to density maps, but which has the potential to extend to other imaging applications. It has a strong mathematical basis that ensures strictly content-based image enhancement. It significantly aids the detectability of dense structures, such as focal densities, masses and calcifications inside mammograms. Focal densities are the key to assess focal asymmetry, which is the core of the new BI-RADS density classification lexicon. RICE works effectively on regular and synthetic mammograms, as well as on SAR and Volpara volumetric density maps. RICE enhances the visibility of focal densities in all Volpara VDG categories (which strongly correlate to BI-RADS breast density classification). In extensive experiments, RICE can consistently unmask tumours falsely embedded in dense breast.

It enhances focal densities by suppressing normal parenchyma, thus reducing the risk of missing cancers that are not visible because it is masked by dense tissue (MISS-1) or its visibility is distracted by other dense tissue (MISS-2). The parenchymal suppression reduces the risk of interpreting cancers wrongly due to overlapping of other tissues (MISS-3).

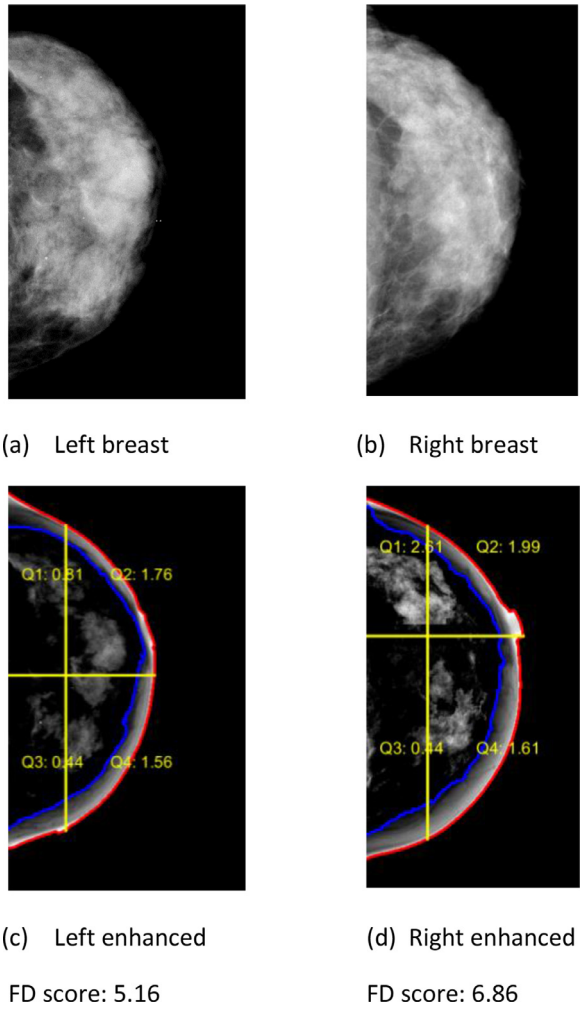

Fig. 23. Quantification of focal density (FD) scores for bilateral mammograms.

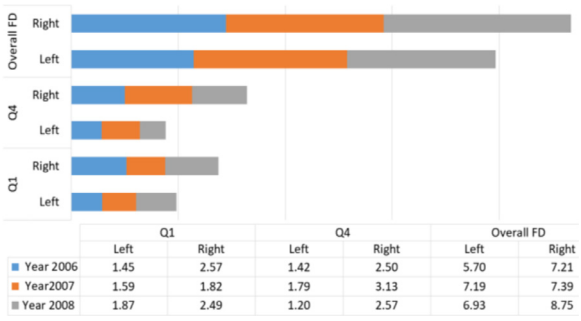

	Q1		Q4		Overall FD	
	Left	Right	Left	Right	Left	Right
Year 2006	1.45	2.57	1.42	2.50	5.70	7.21
Year2007	1.59	1.82	1.79	3.13	7.19	7.39
Year 2008	1.87	2.49	1.20	2.57	6.93	8.75

Fig. 24. Focal density analysis on time series data using our method, confirming the laterality of cancer (right).

Though we are aware of the impressive contributions that deep learning have made generally to (medical) image analysis, it is not a panacea nor does it (or can it) replace everything that has been done using previously developed methods. Of course, there have recently been a stream of exciting papers applying machine learning to mammography, for example by Rodriguez and colleagues (Carioli et al., 2017; Rodríguez-Ruiz et al., 2019; Sasaki et al., 2020) regarding *Transpara* (Le et al., 2019)

A fundamental challenge of applying deep learning to the problem at hand is the small size of carefully curated databases for which "ground truth" (with the consensus view of a number of

informed observers) is available. It has been claimed, and repeatedly reasserted, that machine learning methods such as U-Net are available in such a case, though this has never been shown formally, and the recent work on Deep Convolution Framelets (Han & Ye, 2018) makes explicit the relationship of methods such as U-Net and the classically understood (discrete) wavelet transform, as well as some of the limitations of U-Net. It will be remiss of us not to explore machine learning as we further develop our work; but this was not the focus of the present study.

The current pipeline is illustrative and each of the steps could be replaced without changing the overall impact. For example, the segmentation method, currently based on SLIC, could be replaced by a deep-learning method. In an extended, retrospective observer study we aim to use our method to predict the laterality of breast cancer before it develops. This will help in localizing the future risk of developing cancer, in particular, those associated with mammographic focal densities, and thus enabling early detection and reducing the mortality rate.

Faraz Janan FHEA is a Senior Lecturer in Computer Vision at the University of Lincoln UK. He did a BS in Electrical Engineering from COMSATS University Islamabad Pakistan; MEng in Information and Intelligence from the University of Liverpool UK; and DPhil in Engineering from the University of Oxford. Janan also worked as a Resarch Associate in the Department of Genetics at the University of Cambridge.

Sir Michael Brady FRS FREng FMedSci FBCS FIEE FAAAI is the Emeritus Professor of Oncological Imaging in the Department of Oncology at the University of Oxford. He completed a BSc and MSc in Mathematics (1966, 1967) then a PhD in Group Theory (1970) at the Australian National University. He has been elected FRS, FREng, FMedSci, and a foreign member of Académie des Sciences. Mike has also founded several start-up companies: Guidance Automation; Guidance Monitoring; Guidance Marine; Mirada Solutions; Volpara Health; Mirada Medical; Optellum; Perspectum; ScreenPoint Medical, as well as being a Director of Dexela; Naitive Technologies; Colwiz; Acuitas Medical; AEA Technology plc. He was Deputy Chairman of Oxford Instruments plc 1994-2014. He has recently stepped down as Interim President of the Mohammed bin Zayed University of AI, Abu Dhabi.

Author statement

Faraz Janan: Conceptualization, Methodology, Mathematical Formulation, Data Curation, Writing- Original draft preparation, Visualization, Investigation, Software, Validation, Formal analysis.

Sir Michael Brady: Direction, Supervision, Methodology, Mathematical Formulation, Resources, Writing- Reviewing and Editing

Declaration of Competing Interest

The authors declare that they have no known competing financial interests or personal relationships that could have appeared to influence the work reported in this paper.

References

Achanta, R., Shaji, A., Smith, K., Lucchi, A., Fua, P., Susstrunk, S., 2010. SLIC Superpixels. EPFL Technical Report 149300 doi:10.1109/TPAMI.2012.120.

Aghaei, F., Mirniaharikandehei, S., Hollingsworth, A.B., Wang, Y., Qiu, Y., Liu, H., Zheng, B., 2017. Exploring a new bilateral focal density asymmetry based image marker to predict breast cancer risk. *Medical Imaging 2017*. Image Perception, Observer Performance, and Technology Assessment doi:10.1117/12.2254073.

Aiello, E.J., Buist, D.S.M., White, E., Porter, P.L, 2005. Association between mammographic breast density and breast cancer tumor characteristics. Cancer Epidemiology Biomarkers and Prevention doi:10.1158/1055-9965.EPI-04-0327.

Akila, K., Jayashree, L.S., Vasuki, A., 2015. Mammographic image enhancement using indirect contrast enhancement techniques - A comparative study. Procedia Computer Science doi:10.1016/j.procs.2015.03.205.

Alonzo-Proulx, O., Mainprize, J.G., Harvey, J.A., Yaffe, M.J., 2019. Investigating the feasibility of stratified breast cancer screening using a masking risk predictor. Breast Cancer Res. doi:10.1186/s13058-019-1179-z.

Astley, S.M., Harkness, E.F., Sergeant, J.C., Warwick, J., Stavrinos, P., Warren, R., Wilson, M., Beetles, U., Gadde, S., Lim, Y., Jain, A., Bundred, S., Barr, N., Reece, V., Brentnall, A.R., Cuzick, J., Howell, T., Evans, D.G., 2018. A comparison of five methods of measuring mammographic density: A case-control study. Breast Cancer Res. doi:10.1186/s13058-018-0932-z.

Bakker, M.F., De Lange, S.V., … Pijnappel, R.M., 2019. Supplemental MRI screening for women with extremely dense breast tissue. *N. Engl. J. Med.* doi:10.1056/NEJMoa1903986.

Ball, J.E., Bruce, L.M., 2007. Digital mammographic Computer Aided Diagnosis (CAD) using adaptive level set segmentation. In: Annual International Conference of the IEEE Engineering in Medicine and Biology - Proceedings doi:10.1109/IEMBS.2007.4353457.

Bartella, L., Liberman, L., Morris, E.A., Dershaw, D.D., 2006. Nonpalpable mammographically occult invasive breast cancers detected by MRI. Am. J. Roentgenol. doi:10.2214/AJR.04.1777.

Bhateja, V., Misra, M., Urooj, S., 2017. Human visual system based unsharp masking for enhancement of mammographic images. Journal of Computational Science doi:10.1016/j.jocs.2016.07.015.

Carioli, G., Malvezzi, M., Rodriguez, T., Bertuccio, P., Negri, E., La Vecchia, C., 2017. Trends and predictions to 2020 in breast cancer mortality in Europe. Breast doi:10.1016/j.breast.2017.06.003.

Chen, S.Der, Ramli, A.R, 2003a. Contrast enhancement using recursive mean-separate histogram equalization for scalable brightness preservation. IEEE Trans. Consum. Electron. doi:10.1109/TCE.2003.1261233.

Chen, S.Der, Ramli, A.R, 2003b. Minimum mean brightness error bi-histogram equalization in contrast enhancement. IEEE Trans. Consum. Electron. doi:10.1109/TCE.2003.1261234.

Cheng, H.D., Xu, H., 2000. A novel fuzzy logic approach to contrast enhancement. Pattern Recognit. doi:10.1016/S0031-3203(99)00096-5.

Chiu, S.Y.H., Duffy, S., Yen, A.M.F., Tabár, L., Smith, R.A., Chen, H.H, 2010. Effect of baseline breast density on breast cancer incidence, stage, mortality, and screening parameters: 25-Year follow-up of a Swedish mammographic screening. Cancer Epidemiology Biomarkers and Prevention doi:10.1158/1055-9965.EPI-09-1028.

Chu, J., Min, H., Liu, L., Lu, W., 2015. A novel computer aided breast mass detection scheme based on morphological enhancement and SLIC superpixel segmentation. Med. Phys. doi:10.1118/1.4921612.

DeSantis, C.E., Ma, J., Goding Sauer, A., Newman, L.A., Jemal, A, 2017. Breast cancer statistics, 2017, racial disparity in mortality by state. CA Cancer J. Clin. doi:10.3322/caac.21412.

Ghosh, K., Brandt, K.R., Reynolds, C., Scott, C.G., Pankratz, V.S., Riehle, D.L., Lingle, W.L., Odogwu, T., Radisky, D.C., Visscher, D.W., Ingle, J.N., Hartmann, L.C., Vachon, C.M., 2012. Tissue composition of mammographically dense and non-dense breast tissue. Breast Cancer Res. Treat. doi:10.1007/s10549-011-1727-4.

Gorgel, P., Sertbas, A., Ucan, O.N., 2010. A wavelet-based mammographic image denoising and enhancement with homomorphic filtering. J. Med. Syst. doi:10.1007/s10916-009-9316-3.

Greer, L.R.N, 2014. The benefits of using synthesized 2D (C-view™) images in breast tomosynthesis exams. Appl. Radiol..

Highnam, R., Brady, M., Yaffe, M.J., Karssemeijer, N., Harvey, J., 2010. Robust breast composition measurement - Volpara™. Lecture Notes in Computer Science (Including Subseries Lecture Notes in Artificial Intelligence and Lecture Notes in Bioinformatics) doi:10.1007/978-3-642-13666-5_46.

Hinton, B., Malkov, S., Avila, J., Fan, B., Joe, B., Kerlikowske, K., Ma, L., Mahmoudzadeh, A., Shepherd, J, 2016. A measure of regional mammographic masking based on the CDMAM phantom. Lecture Notes in Computer Science (Including Subseries Lecture Notes in Artificial Intelligence and Lecture Notes in Bioinformatics) doi:10.1007/978-3-319-41546-8_66.

Holland, K., van Gils, C.H., Mann, R.M., Karssemeijer, N., 2017. Quantification of masking risk in screening mammography with volumetric breast density maps. Breast Cancer Res. Treat. doi:10.1007/s10549-017-4137-4.

Hong, B.-W., Brady, M., 2003. Segmentation of mammograms in topographic approach.

Jain, A.K., Farrokhnia, F., 1991. Unsupervised texture segmentation using Gabor filters. *Pattern Recognition* doi:10.1016/0031-3203(91)90143-S.

Jain, A., Singh, S., Bhateja, V., 2013. A robust approach for denoising and enhancement of mammographic images contaminated with high density impulse noise. International Journal of Convergence Computing doi:10.1504/ijconvc.2013.054659.

Janan, F., Brady, M., Highnam, R., 2014. False positive reduction in CADe using diffusing scale space. Lecture Notes in Computer Science (including subseries Lecture Notes in Artificial Intelligence and Lecture Notes in Bioinformatics): Vol. 8539 LNCS doi:10.1007/978-3-319-07887-8_83.

Janan, Faraz, Brady, M., 2015. Shape Description and Matching Using Integral Invariants on Eccentricity Transformed Images. Int. J. Comput. Vision doi:10.1007/s11263-014-0773-x.

Janan, Faraz, Brady, M., Highnam, R., 2015. RICE: Region of Interest Contrast Enhancement of Mammographic Density Maps. In: Proceedings of the 3rd MICCAI Workshop on Breast Image Analysis MICCAI-BIA, p. 129.

Janan, Faraz, Brady, S.M., 2013. Integral invariants for image enhancement. In: Proceedings of the Annual International Conference of the IEEE Engineering in Medicine and Biology Society. EMBS doi:10.1109/EMBC.2013.6610426.

Ji, T.L., Sundareshan, M.K., Roehrig, H., 1994. Adaptive image contrast enhancement based on human visual properties. IEEE Trans. Med. Imaging doi:10.1109/42.363111.

Kim, Y.T., 1997. Contrast enhancement using brightness preserving bi-histogram equalization. IEEE Trans. Consum. Electron. doi:10.1109/30.580378.

Kodinariya, T.M., Makwana, P.R., 2013. Review on determining number of Cluster in K-Means Clustering. International Journal of Advance Research in Computer Science and Management Studies.

Laine, A.F., Schuler, S., Fan, J., Huda, W., 1994. Mammographic Feature Enhancement by Multiscale Analysis. IEEE Trans. Med. Imaging doi:10.1109/42.363095.

Laine, A.F., Zong, X, 1996. Multiscale suboctave wavelet transform for denoising and enhancement. In M. A. Unser, A. Aldroubi, & A. F. Laine (Eds.). Wavelet Applications in Signal and Image Processing IV 2825, 238–249. doi:10.1117/12.255235, SPIE.

Le, E.P.V., Wang, Y., Huang, Y., Hickman, S., Gilbert, F.J, 2019. Artificial intelligence in breast imaging. Clinical Radiology doi:10.1016/j.crad.2019.02.006.

Lee, H.N., Sohn, Y.M., Han, K.H., 2015. Comparison of mammographic density estimation by Volpara software with radiologists' visual assessment: Analysis of clinical-radiologic factors affecting discrepancy between them. Acta Radiol. doi:10.1177/0284185114554674.

Li, H., Liu, K.J.R., Lo, S.C.B, 1997. Fractal modeling and segmentation for the enhancement of microcalcifications in digital mammograms. IEEE Trans. Med. Imaging doi:10.1109/42.650875.

Longo, D.L., 2019. Detecting breast cancer in women with dense breasts. In *New England Journal of Medicine* doi:10.1056/NEJMe1912943.

Lucht, R., Knopp, M.V., Brix, G., 2000. Elastic matching of dynamic MR mammographic images. Magn. Reson. Med. https://doi.org/10.1002/(SICI)1522-2594(200001)43:1<9::AID-MRM2>3.0.CO;2-C.

Lure, F. Y. M., Jones, P. W., & Gaborski, R. S. (1996). Multiresolution unsharp masking technique for mammogram image enhancement. In M.H. Loew & K.M. Hanson (Eds.), Medical Imaging 1996: Image Processing (Vol. 2710, pp. 830–839). SPIE. https://doi.org/10.1117/12.237989

Mainprize, J.G., Alonzo-Proulx, O., Alshafeiy, T.I., Patrie, J.T., Harvey, J.A., Yaffe, M.J., 2019. Prediction of Cancer Masking in Screening Mammography Using Density and Textural Features. Acad. Radiol. doi:10.1016/j.acra.2018.06.011.

Mainprize, J.G., Alonzo-Proulx, O., Alshafeiy, T., Patrie, J.T., Harvey, J.A., Yaffe, M.J., 2018. Masking risk predictors in screening mammography. In: Krupinski, E.A. (Ed.), 14th International Workshop on Breast Imaging (IWBI 2018), 10718. SPIE, pp. 89–94. doi:10.1117/12.2318074.

Mainprize, J.G., Alonzo-Proulx, O., Jong, R.A., Yaffe, M.J., 2016. Quantifying masking in clinical mammograms via local detectability of simulated lesions. Med. Phys. doi:10.1118/1.4941307.

Mainprize, J.G., Wang, X., Ge, M., Yaffe, M.J., 2014. Towards a quantitative measure of radiographic masking by dense tissue in mammography. Lecture Notes in Computer Science (Including Subseries Lecture Notes in Artificial Intelligence and Lecture Notes in Bioinformatics) doi:10.1007/978-3-319-07887-8_26.

Manay, S., Cremers, D., Hong, B.W., Yezzi, A., Soatto, S., 2006. Integral invariants and shape matching. Modeling and Simulation in Science, Engineering and Technology doi:10.1007/0-8176-4481-4_6.

Matsuyama, E., Tsai, D.Y., Lee, Y., Tsurumaki, M., Takahashi, N., Watanabe, H., Chen, H.M., 2013. A modified undecimated discrete wavelet transform based approach to mammographic image denoising. J. Digit. Imaging doi:10.1007/s10278-012-9555-6.

Mencattini, A., Salmeri, M., Lojacono, R., Frigerio, M., Caselli, F., 2008. Mammographic images enhancement and denoising for breast cancer detection using dyadic wavelet processing. IEEE Trans. Instrum. Meas. doi:10.1109/TIM.2007.915470.

Moradmand, H., Setayeshi, S., Karimian, A.R., Sirous, M., Akbari, M.E., 2012. Comparing the performance of image enhancement methods to detect microcalcification clusters in digital mammography. Iranian Journal of Cancer Prevention.

Morar, A., Moldoveanu, F., Gröller, E., 2012. Image segmentation based on active contours without edges. In: 2012 IEEE 8th International Conference on Intelligent Computer Communication and Processing, pp. 213–220. doi:10.1109/ICCP.2012.6356188.

Morrow, W.M., Paranj, R.B., Rangayyan, R.M., Leo Desautels, J.E., 1992. Region-Based Contrast Enhancement of Mammograms. IEEE Trans. Med. Imaging doi:10.1109/42.158944.

Ng, K.H., Lau, S., 2015. Vision 20/20: Mammographic breast density and its clinical applications. Med. Phys. doi:10.1118/1.4935141.

Peart, O., 2014. Positioning challenges in mammography. Radiol. Technol. 85 417M-39M.

Pisano, E.D., Cole, E.B., Hemminger, B.M., Yaffe, M.J., Aylward, S.R., Maidment, A.D.A., Johnston, R.E., Williams, M.B., Niklason, L.T., Conant, E.F., Fajardo, L.L., Kopans, D.B., Brown, M.E., Pizer, S.M, 2000. Image processing algorithms for digital mammography: A pictorial essay. Radiographics doi:10.1148/radiographics.20.5.g00se311479.

Pizer, S.M., Amburn, E.P., Austin, J.D., Cromartie, R., Geselowitz, A., Greer, T., ter Haar Romeny, B., Zimmerman, J.B., Zuiderveld, K., 1987. ADAPTIVE HISTOGRAM EQUALIZATION AND ITS VARIATIONS. *Computer Vision, Graphics, and Image Processing* doi:10.1016/S0734-189X(87)80186-X.

Popli, M.B., Teotia, R., Narang, M., Krishna, H., 2014. Breast positioning during mammography: Mistakes to be avoided. Breast Cancer: Basic and Clinical Research doi:10.4137/BCBCr.s17617.

Rangayyan, R.M., Shen, L., Shen, Y., Leo Desautels, J.E., Bryant, H., Terry, T.J., Horeczko, N., Sarah Rose, M., 1997. Improvement of sensitivity of breast cancer diagnosis with adaptive neighborhood contrast enhancement of mammograms. IEEE Trans. Inf. Technol. Biomed. doi:10.1109/4233.654859.

Rodríguez-Ruiz, A., Krupinski, E., Mordang, J.J., Schilling, K., Heywang-Köbrunner, S.H., Sechopoulos, I., Mann, R.M., 2019. Detection of breast cancer with mammography: Effect of an artificial intelligence support system. Radiology doi:10.1148/radiol.2018181371.

Romualdo, L.C.S., Vieira, M.A.C., Schiabel, H., Mascarenhas, N.D.A., Borges, L.R, 2013. Mammographic image denoising and enhancement using the anscombe transformation, adaptive wiener filtering, and the modulation transfer function. J. Digit. Imaging doi:10.1007/s10278-012-9507-1.

Salmeri, M., Mencattini, A., Rabottino, G., Accattatis, A., Lojacono, R., 2008. Signal-dependent noise characterization for mammographic images denoising. In: 16th IMEKO TC4 Int. Symp.: Exploring New Frontiers of Instrum. and Methods for Electrical and Electronic Measurements; 13th TC21 Int. Workshop on ADC Modelling and Testing - Joint Session *Proc.*.

Sasaki, M., Tozaki, M., Rodríguez-Ruiz, A., Yotsumoto, D., Ichiki, Y., Terawaki, A., Oosako, S., Sagara, Y., Sagara, Y., 2020. Artificial intelligence for breast cancer detection in mammography: experience of use of the ScreenPoint Medical Transpara system in 310 Japanese women. Breast Cancer doi:10.1007/s12282-020-01061-8.

Scharcanski, J., Jung, C.R., 2006. Denoising and enhancing digital mammographic images for visual screening. Comput. Med. Imaging Graph. doi:10.1016/j.compmedimag.2006.05.002.

Schreer, I., 2009. Dense breast tissue as an important risk factor for breast cancer and implications for early detection. Breast Care doi:10.1159/000211954.

Sergeant, J.C., Warwick, J., Gareth Evans, D., Howell, A., Berks, M., Stavrinos, P., Sahin, S., Wilson, M., Hufton, A., Buchan, I., Astley, S.M., 2012. Volumetric and area-based breast density measurement in the predicting risk of cancer at screening (PROCAS) study. Lecture Notes in Computer Science (Including Subseries Lecture Notes in Artificial Intelligence and Lecture Notes in Bioinformatics) doi:10.1007/978-3-642-31271-7_30.

Siegel, R.L., Miller, K.D., Jemal, A., 2015. Cancer statistics 2015. CA Cancer J. Clin. doi:10.3322/caac.21254.

Siegel, R.L., Miller, K.D., Jemal, A., 2020. Cancer statistics, 2020. CA Cancer J. Clin. doi:10.3322/caac.21590.

Sivaramakrishna, R., Obuchowski, N.A., Chilcote, W.A., Cardenosa, G., Powell, K.A., 2000. Comparing the performance of mammographic enhancement algorithms: A preference study. Am. J. Roentgenol. doi:10.2214/ajr.175.1.1750045.

Spak, D.A., Plaxco, J.S., Santiago, L., Dryden, M.J., Dogan, B.E., 2017. BI-RADS® fifth edition: A summary of changes. Diagnostic and Interventional Imaging doi:10.1016/j.diii.2017.01.001.

Srinath, M.D., 1992. Conjugate Gradient Techniques for Adaptive Filtering. IEEE Transactions on Circuits and Systems I: Fundamental Theory and Applications doi:10.1109/81.109237.

Tabár, L., Dean, P.B., 1982. Mammographic parenchymal patterns. JAMA 247 (2), 185–189.

Tabár, L., Vitak, B., Chen, T.H.H., Yen, A.M.F., Cohen, A., Tot, T., Chiu, S.Y.H., Chen, S.L.S., Fann, J.C.Y., Rosell, J., Fohlin, H., Smith, R.A., Duffy, S.W, 2011. Swedish two-county trial: Impact of mammographic screening on breast cancer mortality during 3 decades. Radiology doi:10.1148/radiol.11110469.

Tang, J., Liu, X., Sun, Q., 2009. A direct image contrast enhancement algorithm in the wavelet domain for screening mammograms. IEEE J. Sel. Top. Sign. Proces. doi:10.1109/JSTSP.2008.2011108.

Teo, I., Whelehan, P., MacAskill, J.E., Vinnicombe, S., Munnoch, D.A., Evans, A., 2016. Volpara™ as a measurement tool for breast volume. Journal of Plastic, Reconstructive and Aesthetic Surgery doi:10.1016/j.bjps.2015.11.024.

Therrian, C.W., 1981. Linear filtering models for terrain image segmentation.

Torre, L.A., Bray, F., Siegel, R.L., Ferlay, J., Lortet-Tieulent, J., Jemal, A., 2015. Global cancer statistics, 2012. CA Cancer J. Clin. doi:10.3322/caac.21262.

Tromans, C.E., Cocker, M.R., Brady, S.M., 2012. Quantification and normalization of x-ray mammograms. Phys. Med. Biol. 57 (20), 6519–6540. doi:10.1088/0031-9155/57/20/6519.

Vala, M., Baxi, A., 2013. A review on Otsu image segmentation algorithm. International Journal of Advanced Research in Computer Engineering & Technology (IJARCET.

Van Goethem, M., Schelfout, K., Dijckmans, L., Van Der Auwera, J.C., Weyler, J., Verslegers, I., Biltjes, I., De Schepper, A., 2004. MR mammography in the preoperative staging of breast cancer in patients with dense breast tissue: Comparison with mammography and ultrasound. European Radiology doi:10.1007/s00330-003-2146-7.

Vedaldi, A., Fulkerson, B., 2010. Vlfeat - An open and portable library of computer vision algorithms. In: MM'10 - Proceedings of the ACM Multimedia 2010 International Conference doi:10.1145/1873951.1874249.

Volumetric, Q., Software, D., 2010. Abridged Clinical Results.

Wang, J., Aziz, A., Newitt, D., Joe, B.N., Hylton, N., Shepherd, J.A., 2012. Comparison of Hologic ' s Quantra Volumetric Assessment to MRI Breast Density 619–626.

Wu, S., Zhu, Q., Yang, Y., Xie, Y., 2013. Feature and contrast enhancement of mammographic image based on multiscale analysis and morphology. 2013 IEEE International Conference on Information and Automation, ICIA 2013 doi:10.1109/ICInfA.2013.6720354.

Zhou, C., & Chan, H. (2001). Computerized image analysis: Estimation of breast density on mammograms. … *York-Institute of* …, 11–13. https://doi.org/10.1118/1.1376640

Zhou, Y., Panetta, K., Agaian, S., 2010. Human visual system based mammogram enhancement and analysis. 2010 2nd International Conference on Image Processing Theory, Tools and Applications, IPTA 2010 doi:10.1109/IPTA.2010.5586759.